

Optical absorption of Mo-based alloys

Madoka Tokumoto

Electrotechnical Laboratory, Sakura-mura, Niihari-gun, Ibaraki 305, Japan

H. D. Drew

Department of Physics and Astronomy, University of Maryland, College Park, Maryland 20742

(Received 2 February 1984; revised manuscript received 1 May 1984)

A study of the optical absorption of Mo-based dilute alloys (*MoRe*, *MoOs*, *MoPt*) by a sensitive differential technique is presented. The experiment is analyzed for the difference in the optical conductivity between the alloy and pure Mo. The structures observed in the differential optical conductivity are classified into two groups: One is sensitive to impurity species and the other is not. The former structures, which appear in the region of photon energy below 2 eV, are found to behave consistently with the prediction of the rigid-band approximation in the framework of the indirect optical transition model. The latter structures, which lie above 2 eV, are shown to be well described in terms of the change in optical conductivity arising from impurity-induced wave-vector-nonconserving optical absorption processes, on the basis of the electronic band-structure calculation of pure molybdenum.

I. INTRODUCTION

In Mo-based alloys (*MoNb*, *MoRe*, etc.) the electronic density of states at the Fermi level determined by electronic heat-capacity measurements is known to show a rigid-band-like behavior.¹ That is, if the experimentally determined density of states at the Fermi level for various Mo-based alloys are plotted as a function of the Fermi energy which is determined by the electron-to-atom ratio (i.e., average number of valence electrons) of the alloys, the data agree well with the theoretical density of states of pure molybdenum. The rigid-band model has been widely applied for the analysis of transport properties of Mo-based alloys.² The applicability of the rigid-band model to the whole electronic structure, however, can only be confirmed by optical or other spectroscopic measurements which probe the electronic structure at energies up to several electron volts above and below the Fermi level, a region untouched by the sophisticated "Fermi-surface" measurements. However, the optical studies to date appear to be insufficient to exclude the applicability of the rigid-band model to Mo-based alloys. Bahl *et al.*³ studied the differential optical reflectivity of Mo-Re alloy and concluded that the rigid-band model is inapplicable to that case. They observed a large peak near 1 eV which they interpreted as arising from localized Re *d* states located in the valley of the host (Mo) density of states between the bonding and antibonding orbital density-of-state peaks. Black *et al.*⁴ measured optical properties of Nb-Mo alloys and concluded that the rigid-band model without inclusion of electric dipole matrix elements can explain the spectra for Nb-rich alloys with Mo in the (1–3)-eV region, but it is poor at higher energies, and for the Mo-rich end of the system. They also concluded that alloying does not cause major changes in optical selection rules. More recently, Colavita *et al.*⁵ measured the thermorefectance of Nb-Mo alloys, and concluded that while

the lower conduction bands behave roughly as predicted by the rigid-band model, the higher-lying conduction bands show distinctly non-rigid-band-like behavior.

In this paper, we present a study of the differential optical properties of *MoRe*, *MoOs*, and *MoPt* alloys, based on an improved sample preparation process compared with the previous work.³ We conclude that the changes in the optical spectra of Mo-rich alloys below 2 eV are consistent with the rigid-band model, while the spectral features at higher energies can be explained in terms of the change in optical selection rules caused by alloying.

II. EXPERIMENTAL

A. Sample preparation

The samples were prepared by simultaneous vacuum evaporation of the two constituents onto polished fused-quartz substrates, 1 mm thick by 25.4 mm diam, preheated to 500°C. Two substrates, one for the alloy and the other for the pure-metal reference samples, were mounted in the evaporation chamber in a geometry such that a shield placed between the two sources prevented the solute vapor from falling onto the pure side substrate while permitting the molybdenum vapor to fall on both. The deposition rates were typically 50 Å/sec (monitored by a quartz oscillator), and the total thickness was typically 3000 Å. The molybdenum was evaporated with a Varian 5-kW electron-beam evaporation source, while the solute (Re, Os, or Pt) was evaporated with a Varian 2-kW electron-beam evaporation source. The evaporation chamber was evacuated by a conventional oil-diffusion pump with a liquid-nitrogen trap. While preheating substrates the pressure in the evaporation chamber was about 5×10^{-7} Torr, which rose to about 5×10^{-6} Torr during film deposition. The solute concentrations were controlled to be around 4 at. % by measuring the ratio of the

deposition rates of host and solute materials, monitored independently by two quartz oscillators. Actual composition, however, may suffer from the variation of sticking coefficient. Details of sample preparation and other experimental conditions were described elsewhere.⁶

B. Reflectivity measurements

Reflectivity measurements were made with a single-beam differential reflectometer similar to that described by Beaglehole.⁷ Both pure-metal and alloy samples were mounted on a rotating holder so that light beam was reflected alternatively from pure molybdenum and an alloy sample. The quantity $\alpha = (R_{\text{pure}} - R_{\text{alloy}}) / (R_{\text{pure}} + R_{\text{alloy}})$ was recorded continuously as a function of photon wavelength. Typical spectra of α versus photon energy are shown in Fig. 1. α was measured to one part in 10^4 in the visible photon wavelength region, and the precision fell off to 1 part in 10^3 in the infrared (below 0.6 eV) and in the ultraviolet (above 5 eV). It was essential that the pure-metal and alloy samples to be measured were prepared at the same time, in order to reduce the reflectivity differences due to variations of vacuum-deposition conditions and the effect of "aging" after exposure to air. The reflectivities of our pure-molybdenum films were measured separately using a Perkin-Elmer model 350 spectrophotometer with a specular-reflectance accessory. We found a reasonable agreement between the reflectivities of our molybdenum films and the published results on bulk samples,⁸ as shown in Fig. 2.

C. Kramers-Kronig inversion

The complex conductivity function $\hat{\sigma} = \sigma_1 + i\sigma_2$ of the sample was obtained through a Kramers-Kronig analysis

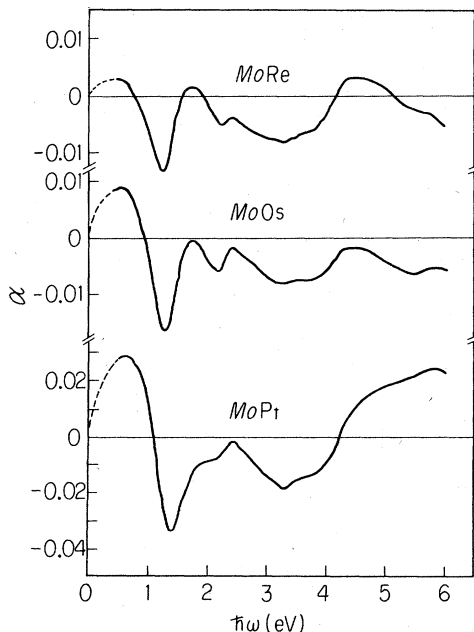


FIG. 1. Experimental data of the differential reflectivity $\alpha = (R_{\text{pure}} - R_{\text{alloy}}) / (R_{\text{pure}} + R_{\text{alloy}})$ measured for MoRe, MoOs, and MoPt alloy films. Alloy concentrations are about 4 at. %.

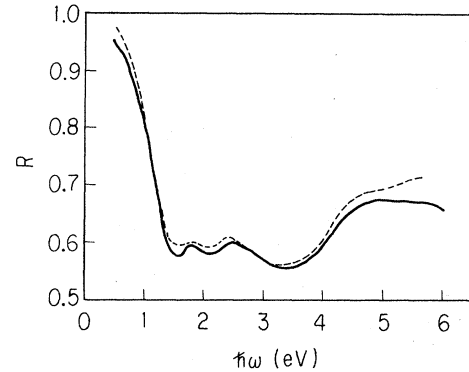


FIG. 2. Optical reflectivity of pure molybdenum. The solid line is the reflectivity data for our pure-Mo film. The dashed line is the reflectivity of Ref. 8 for bulk Mo.

of the reflectivity data. $\hat{\sigma}_{\text{pure}}$ and $\hat{\sigma}_{\text{alloy}}$ were determined separately from R_{pure} and $R_{\text{alloy}} = R_{\text{pure}}[(1-\alpha)/(1+\alpha)]$. The results were then presented in terms of the differential conductivity $\Delta\sigma_1 = \sigma_1^{\text{alloy}} - \sigma_1^{\text{pure}}$. As always, in performing the Kramers-Kronig analysis, it was necessary to extrapolate the reflectivity data outside the measured spectral range.

For the low-energy extrapolation, we modeled the complex dielectric function $\hat{\epsilon} = 1 + 4\pi i\hat{\sigma}/\omega$ as the sum of a Drude term for the conduction-electron response and a simple Lorentzian oscillator term to account in an appropriate way for the interband absorption. The oscillator frequency ω_L was located well above the low-frequency cutoff ω_1 at 0.5 eV. Thus, for the low-energy extrapolation, we have

$$\hat{\epsilon}(\omega) = 1 - \frac{\omega_p^2}{\omega(\omega + i/\tau_{\text{opt}})} + \frac{f_L}{\omega_L^2 - \omega^2 - i\Gamma\omega}, \quad \omega < \omega_1. \quad (1)$$

For the Drude term we used the plasma frequency ($\omega_p = 7.9$ eV) given by Veal and Paulikas⁸ for pure molybdenum, and the small change expected for the alloy was ignored since it could not be reliably determined by our parametrization. The lifetime τ_{opt} and the three parameters (ω_L , f_L , and Γ) in the Lorentz oscillator term were then determined by a weighted least-squares fit to the reflectivity data near the low-frequency cutoff. This procedure was found to provide a physically consistent low-energy extrapolation. Representative values for the low-energy extrapolation parameters are given in Table I as well as the dc relaxation time τ_{dc} , evaluated from the residual resistivity ratio (\mathcal{R}), using the relation

$$\frac{\hbar}{\tau_{\text{dc}}} \approx \frac{(\hbar\omega_p)^2}{4\pi\hbar\sigma_0(\text{rt})} \frac{\mathcal{R}}{\mathcal{R} - 1} \quad (2)$$

where $4\pi\hbar\sigma_0(\text{rt}) = 1304$ eV corresponding to the dc resistivity $\rho_0 = 5.7$ Ω cm of bulk molybdenum at room temperature. The optically estimated values of τ_{opt} are consistently smaller than the dc values, and they show a consistent variation from one alloy to the other as expected. The Lorentz oscillator term was necessary in order to obtain a smooth extrapolation with reasonably small values of \hbar/τ_{opt} . The resultant $\Delta\sigma_1$'s were not very sensitive to

TABLE I. Representative values for the residual resistivity ratio (\mathcal{R}), dc relaxation time, and parameters for low- and high-energy extrapolations of reflectivity.

	\mathcal{R}	$\frac{1}{\tau_{dc}}$ (eV)	$\frac{1}{\tau_{opt}}$ (eV)	ω_L (eV)	f_L (eV ²)	Γ (eV)	ω_0 (eV)
pure Mo	3.8	0.07	0.14	1.8	126	2.8	13.2
Mo _{0.96} Re _{0.04}	2.5	0.08	0.16	2.5	260	6.2	13.2
Mo _{0.96} Os _{0.04}	2.0	0.10	0.20	2.0	184	4.8	13.3
Mo _{0.96} Pt _{0.04}	1.3	0.21	0.30	2.6	435	10.4	13.7

this low-energy extrapolation, except very near the cutoff frequency.

We extrapolated our reflectivity data for pure molybdenum samples to higher energy ($\hbar\omega > 6.0$ eV) as follows. We approximated the reflectance by

$$R(\omega) = R(\omega_h) \left[\frac{\omega_h^2 + \omega_0^2}{\omega^2 + \omega_0^2} \right]^{p/2}, \quad \omega > \omega_h, \quad p > 0, \quad (3)$$

where ω_h is the frequency of the highest measured point at 6.0 eV, and ω_0 and p are parameters. We have found that it is adequate to represent reflectivity with $p=4$ in Eq. (3) at frequencies where some contribution from interband transitions still remains, since it smoothly reduces to the free-electron asymptotic limit $R(\omega) \propto \omega^{-4}$ for sufficiently high frequency ($\omega \gg \omega_0$). The parameter ω_0 was chosen to be 13 eV so that the Kramers-Kronig inverted optical conductivity, $\sigma_1(\omega) = \omega\epsilon_2(\omega)/4\pi$, matched the ellipsometric data by Kirillova *et al.*⁹ around 2 eV, where ellipsometry is considered to be most reliable. (With $\omega_0=0$ we obtain $p=2$, which is unphysical, in order to satisfy the same requirement.)

$\sigma_1(\omega)$ obtained in this manner for the pure-Mo film is shown in Fig. 3. The dashed line in Fig. 3 shows the Drude contribution to the optical conductivity σ_1^D , calculated using the low-energy extrapolation parameters described above. The remaining interband contribution, σ_1^{ib} , is shown by the dashed-dotted line.

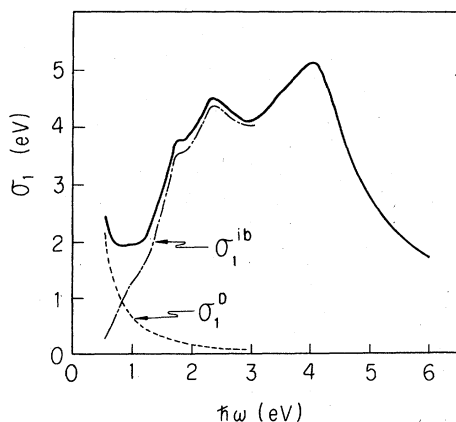


FIG. 3. Optical conductivity of pure molybdenum. The solid line was obtained from Kramers-Kronig inversion of the measured reflectivity using extrapolations described in the text. The dashed line represents a Drude contribution as used for the low-energy extrapolation of the reflectivity, and the dashed-dotted line corresponds to the interband optical conductivity.

For alloy samples we modified the extrapolation parameter ω_0 in order to satisfy the differential conductivity sum rule

$$\Delta n = \frac{2m}{\pi e^2} \int_0^{\omega_s} \Delta\sigma_1(\omega') d\omega', \quad (4)$$

where Δn is the difference of the density of valence electrons between pure molybdenum and alloys. The high-frequency cutoff ω_s in Eq. (4) was taken to be the frequency for the saturation of the conductivity sum rule for valence electrons in the pure system. We obtained a reasonable result of $\omega_s = 60$ eV, indicating that the oscillator strength of the six valence electrons in molybdenum (atomic configuration $4d^5 5s^1$) is exhausted at this energy. The high-energy parameters have a large influence on the magnitude of the resultant differential optical conductivity. The spectral features, however, are much less sensitive to the choice of the extrapolation parameters. The representative values for the high-energy extrapolation parameters are also given in Table I.

III. DISCUSSION

The results for $\Delta\sigma_1$ for *MoRe*, *MoOs*, and *MoPt* are shown in Fig. 4. We note and discuss the following spectral features in this section. First, the low-energy part (below 1.5 eV) contains a sharply rising low-frequency divergence in common. The second feature of interest is the various structures around 2 eV. Finally, at higher frequencies, there is a pronounced dip at 4.1 eV which is commonly seen for all three kinds of alloys with different impurity species.

First of all, we will discuss the so-called Drude contribution caused by the change of the free-electron absorption upon alloying. The low-frequency divergence in $\Delta\sigma_1$ can be interpreted largely in terms of the increased scattering of the conduction electrons in alloys. At the frequencies where $\omega \gg 1/\tau_{alloy} > 1/\tau_{pure}$, the Drude contribution to $\Delta\sigma_1$ can be approximately expressed as

$$\Delta\sigma_1 \approx \frac{1}{4\pi} \left[\frac{1}{\tau_{alloy}} - \frac{1}{\tau_{pure}} \right] \frac{\omega_p^2}{\omega^2}, \quad (5)$$

which gives a positive low-frequency divergence in $\Delta\sigma_1$ as observed experimentally. The value of Eq. (5) for each alloy, calculated using parameters in Table I, is plotted in Fig. 4 by the dashed line. A larger Drude contribution for *MoPt* in Fig. 4 corresponds to shorter τ_{alloy} in Table I.

Secondly, we will discuss the interband contribution which is usually complicated in transition-metal-based al-

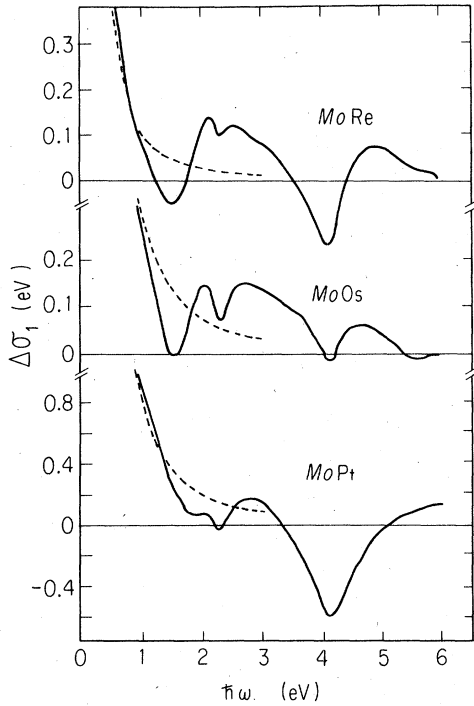


FIG. 4. Differential optical conductivity $\Delta\sigma_1 = \sigma_1^{\text{alloy}} - \sigma_1^{\text{pure}}$ obtained by Kramers-Kronig analysis of data in Fig. 1. The dashed lines correspond to Drude contributions given by Eq. (5).

loys due to the presence of complex d bands with plenty of structures in the density of states within the spectral region of interest. In the course of optical studies on Ni-based alloys, we have pointed out the important role of impurity-induced indirect transitions, i.e., wave-vector-nonconserving transitions.^{6,10} We now examine whether the same indirect optical processes can explain any part of the spectral features in $\Delta\sigma_1$. In the following discussion, we will utilize the results of the calculation of the optical conductivity of molybdenum by Koelling, Mueller, and Veal.¹¹ The calculation was based on the band-structure computation by means of the relativistic augmented-plane-wave method. Two theoretical models based on the band approximation were employed for the calculation of the optical conductivity. The first, or direct-transition, model ignores lifetime effects and assumes that wave-vector (\vec{k}) conservation is an important selection rule, while the second one, called the indirect model, emphasizes such lifetime effects, ignores selection rules, and depends on transition energies alone. In the indirect model, assuming constant matrix elements, the interband part of $\sigma_1(\omega)$ was found for the density of states as

$$\sigma_1(\omega) \propto \frac{1}{\omega} \int_{E_F}^{E_F + \hbar\omega} n_f(E) n_i(E - \hbar\omega) dE. \quad (6)$$

Here n_f and n_i , respectively, refer to final- and initial-state densities about E_F . In the direct-transition model (interband absorption only), $\sigma_1(\omega)$ is given by

$$\sigma_1(\omega) = \sum_{f,i} m^2 \hbar \frac{e^2}{\omega} \int |M_{fi}(\vec{k}, \omega)|^2 \delta(E_{fi} - \hbar\omega) d\vec{k}, \quad (7)$$

where i, f designate band indices for filled initial and empty final states, respectively, $E_{fi} = E_f - E_i$, and the matrix elements are given by $|M_{fi}(\vec{k}, \omega)|^2 = |\langle \psi_f | \hat{\epsilon} \cdot \vec{p} | \psi_i \rangle|^2$ in the nonrelativistic approximation. Figure 5 shows the $\sigma_1(\omega)$'s computed by Koelling *et al.* for the direct-transition model using constant-matrix elements (dashed line), and the indirect model (dashed-dotted line) along with the experimental results (solid line) from Ref. 11. In order to see what we should expect for $\Delta\sigma_1$ corresponding to the disorder-induced wave-vector-nonconserving optical absorption, we evaluate two quantities as a function of photon energy in Fig. 6; that is, (a) the difference between the results of indirect- and direct-transition model calculations, $\Delta\sigma_1 = \sigma_1(\text{indirect}) - \sigma_1(\text{direct})$, and (b) the difference between the indirect-transition model calculation and the experimental result, $\Delta\sigma_1 = \sigma_1(\text{indirect}) - \sigma_1(\text{experiment})$. The meaning of the latter quantity, (b) may not appear as straightforward as the former one, (a). The indirect model completely neglects the wave-vector-conservation selection rule, whereas the actually observed optical conductivity of pure metal is expected to be governed to some extent by the selection rule, including direct processes. After introduction of a small number of impurity atoms, we have "nearly direct" transitions—the wave vector has still some meaning. It is not a total rejection of the direct process implied by the convolution integral in the indirect process. Nevertheless we can still expect that the difference between the calculated $\sigma_1(\text{indirect})$ and experimental $\sigma_1(\text{pure})$ would suggest how and to what extent the optical conductivity could change when the selection rule is relaxed upon introduction of impurity atoms. Since (a) is regarded more complete and consistent in the framework of the theoretical consideration, as compared with (b) which is a semiempirical mixture of theory and experi-

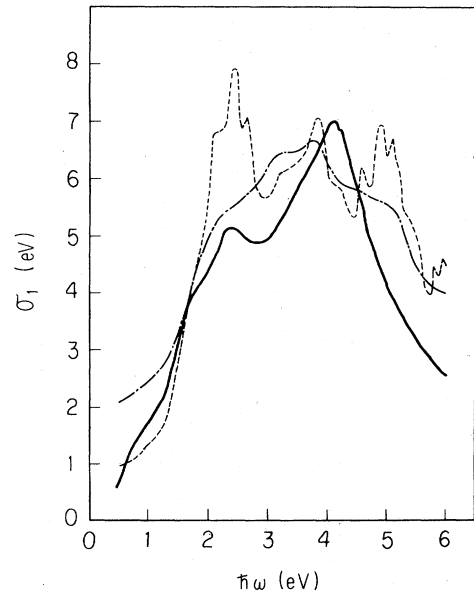


FIG. 5. Interband optical conductivity of molybdenum, from Ref. 11. The dashed line is a theoretical calculation based on the direct model, using a constant-matrix element, and the dashed-dotted line is based on the indirect model. The solid line is experimental data.

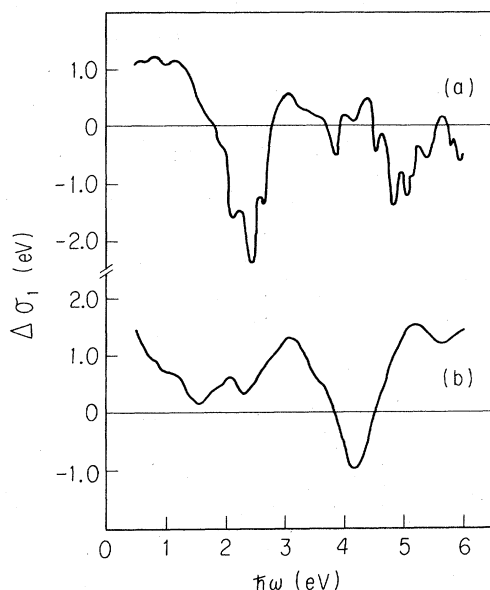


FIG. 6. Differences in optical conductivity calculated using σ_1 's in Fig. 5. (a) $\Delta\sigma_1 = \sigma_1(\text{indirect}) - \sigma_1(\text{direct})$ (b) $\Delta\sigma_1 = \sigma_1(\text{indirect model}) - \sigma_1(\text{experiment})$. These quantities are related to the change in optical-absorption spectra caused by the introduction of disorder by alloying.

ment, one naturally expects that (a) should work better than (b). However, upon comparison of $\Delta\sigma_1$ in Fig. 6 with those in Fig. 4, one clearly sees that (b) in Fig. 6 reproduces the experimental spectral features (a pronounced dip at 4.1 eV and a smaller one at 2.2 eV) in Fig. 4 surprisingly well, while (a) in Fig. 6 does not. This unexpected result can be understood as follows.

(i) The present one-electron energy-band calculation gives sufficiently reliable results: The indirect model based on the density of states alone reflects properly the case when the wave-vector conservation rule is completely ignored.

(ii) The direct model, on the other hand, does not satisfactorily reproduce the overall spectral features in the measured optical conductivity of molybdenum.

The second point does not necessarily mean that the direct model itself is as unsatisfactory as it appears to be. Dipole matrix elements are notoriously difficult to calculate accurately, and the problem is likely to lie in the matrix elements.¹² It is also recognized that, so far, the features at 4.1 eV in Mo and 4.5 eV in Ni which are the most prominent in the optical response are not well understood from the band theory.^{11,13} Inclusion of dynamical correlation may possibly improve the existing band-structure calculations.¹⁴

It is to be noted that a model calculation of the quantity similar to the above (b) has been shown to explain $\Delta\sigma_1$ spectra in Ni-based alloys also.¹⁰ A difference, however, exists since the impurity-induced optical absorption resulted in a positive $\Delta\sigma_1$ peak at 2 eV and a broad $\Delta\sigma_1$ dip around 4.5 eV in the case of Ni-based alloys, whereas we only have dips or negative peaks in $\Delta\sigma_1$ for Mo-based al-

loys. The positive $\Delta\sigma_1$ peak at 2 eV in Ni-based alloy corresponds to a pronounced peak in the optical conductivity in the indirect model calculation, or more specifically, in the calculated joint density of states in the minority-spin band.¹⁰ Absence of a corresponding peak in the measured conductivity of pure Ni implies that the indirect transitions are suppressed by the dipole selection rule, which can be relaxed by the introduction of disorder. This interpretation leads to a positive $\Delta\sigma_1$ peak at 2 eV as well as a negative $\Delta\sigma_1$ background elsewhere to obtain a system sum rule. The negative $\Delta\sigma_1$ peak around 4.5 eV in Ni-based alloys seems to have a common origin with the negative $\Delta\sigma_1$ peaks in Mo-based alloys. The fact that these peaks are negative implies that they are related to the reduction of host σ_1 . The reduction of the optical conductivity of the host can come about for two reasons. One is the decrease in host atoms, and a simple reduction proportional to the host σ_1 has been proposed.¹⁵ But this carries with it the implication that the transitions are localized on the host atoms. The other is a selective reduction of the preexisting direct optical transitions. As we saw, the direct transition model did not successfully fit the experimental optical conductivity as a whole in the case of pure Mo, but this does not exclude the possibility that direct transition processes are involved somewhere in the measured spectrum. Here we assume the existence of direct optical transitions at 2.2 and 4.0 eV in the optical conductivity spectrum of pure Mo. If we have direct transitions and introduce some scattering centers, but not many, it seems we can simulate the effect by increasing the relaxation rate. This is what happens in the coherent potential approximation (CPA) calculations—the bands attain finite width from the imaginary part of the self-energy. In this case we have broadening of the direct transition peak, which results in a decrease in the optical conductivity at the peak energy as well as a smaller increase around. A closer look reveals that, actually, optical transitions in pure Mo consist mainly of wave-vector-conserving direct transitions at these photon energy where we observe dips in $\Delta\sigma_1$. Since these direct transitions are relatively suppressed by the introduction of disorder, while the rest of the σ_1 spectrum grows at large, we apparently have negative peaks or dips in $\Delta\sigma_1$ at these photon energies. This argument can be substantiated by identifying the nature of these optical transitions, as follows. According to Koelling *et al.*,¹¹ a weak shoulder in σ_1 appearing at 2.2 eV results from direct transitions from band 5 to band 6 along Δ (transitions from the "lens" of the Fermi surface). Also a pronounced peak at 4.0 eV in σ_1 results from a direct Fermi-level transition along Δ . Moreover, the absorption peak near 4.0 eV should persist with the inclusion of matrix elements. The 4.0-eV peak, attributed primarily to transitions from bands 3,4 to band 6 near Δ , results from transitions originating at *s* bands, which are strongly hybridized with overlapping *d* bands, and terminating at *d* bands. The hybridized band has a significant fraction of *p* character with the result that the dipole selection rules for the 4.0-eV peak should be reasonably well satisfied.

Therefore, as a result of the above comparison, the origin of the pronounced dip in $\Delta\sigma_1$ at 4.1 eV and a smaller

dip at 2.2 eV, which are commonly seen in Fig. 4, can be unambiguously ascribed to the effect of the impurity-induced-indirect optical transitions.

To see additional evidence for the impurity-induced-indirect transition and to examine the possibility of interpreting the spectral features below 2 eV in terms of the rigid-band model, the experimental result on optical properties of Mo-Nb alloys by Black *et al.*⁴ is useful. In Fig. 7, the solid line reproduces a part of their difference spectra for $\Delta\sigma_1 = \sigma_1(\text{Mo}_{0.8}\text{Nb}_{0.2}) - \sigma_1(\text{Mo})$. First, it should be noted that similar spectral features to our $\Delta\sigma_1$, i.e., pronounced dip at 4.1 eV and a smaller one at 2.2 eV, were observed irrespective of different impurity species. Secondly, the spectral features of $\Delta\sigma_1$ below 2 eV, on the other hand, seem to be sensitive to impurity species, indicating that this low-energy portion of the $\Delta\sigma_1$ spectra is caused by different mechanisms.

We next examine what the rigid-band model predicts for the optical properties of this alloy system. The rigid-band model calculation by Pickett and Allen¹⁶ for the case of 20 at. % Nb in Mo is plotted by the dashed line in Fig. 7. Upon comparison with the experiment, we must admit that the negative conclusion by Black *et al.* is inappropriate.¹⁷ Actually, as is shown in Fig. 7, the rigid-band model calculation by Pickett and Allen reasonably explains the spectral features of the measured $\Delta\sigma_1$ below 2 eV. Interestingly, a similar comparison for $\Delta\sigma_1 = \sigma_1(\text{Nb}_{0.8}\text{Mo}_{0.2}) - \sigma_1(\text{Nb})$ also shows reasonable agreement between theory and experiment. Thus the agreement between measured and calculated differences in optical conductivity is found to be much better than concluded in Ref. 4 at both the Mo-rich and Nb-rich ends of the system.

Another useful test of the rigid-band model is as follows. As was discussed by Beaglehole and Hendrickson,¹⁵ if $\Delta(\hbar\omega)$ is an energy shift, then a $\Delta\sigma_1 = -[d\sigma_1^{\text{ib}}/d(\hbar\omega)]\Delta(\hbar\omega)$ will result. Figure 8 shows $d\sigma_1^{\text{ib}}/d(\hbar\omega)$ for pure Mo. We are now concerned with a $d\sigma_1^{\text{ib}}/d(\hbar\omega)$ peak around 1.5 eV in Fig. 8, which is related to the absorption edge near 1.5 eV in Fig. 3. According to Koelling *et al.*,¹¹ the abrupt absorption edge near 1.5 eV is present in both direct and indirect models. For the indirect model, the edge largely results from a peak in the density of states about 1.5 eV below E_F coming from the region of the Brillouin zone near Γ . For the direct model, transi-

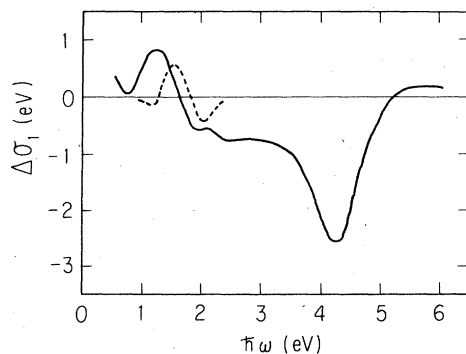


FIG. 7. Differences in optical conductivity $\Delta\sigma_1 = \sigma_1(\text{Mo}_{0.8}\text{Nb}_{0.2}) - \sigma_1(\text{pure Mo})$ as measured (solid line) in Ref. 4, and calculated (dashed line) in Ref. 12.

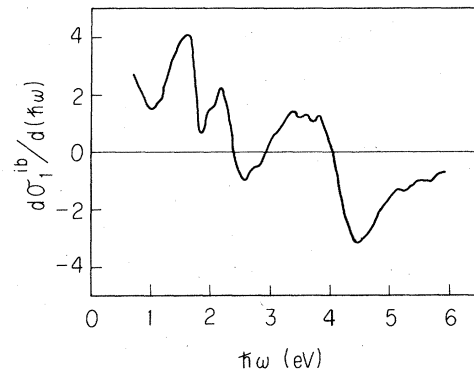


FIG. 8. First derivative of the interband optical conductivity of molybdenum calculated using the dashed-dotted line in Fig. 3.

tions from this peak in $n_i(E)$ are not so important. However, additional large contributions come to $\sigma_1(\omega)$ at this energy from transitions between bands along Δ (also bands along Σ) which are nearly parallel over an extended region of the Brillouin zone. Upon alloying with Re or Os, additional electron density shifts the Fermi surface to higher energy in the rigid-band model. Thus in the indirect model a transition to the Fermi level would show a distinct blue shift and therefore a negative $\Delta\sigma_1$ peak near 1.5 eV. On the other hand, in the direct model, transitions between nearly parallel bands predict only a small red shift and thus a small positive $\Delta\sigma_1$ peak near 1.5 eV. The observed negative peak in $\Delta\sigma_1$ at about 1.5 eV in Fig. 4 for *MoRe* and *MoOs* is consistent with the rigid-band picture if the indirect-transition model is applicable.¹⁸ It would also be helpful to look into the case where the electron density is reduced upon alloying with elements located on the opposite side of the Periodic Table. Since experimental efforts to obtain optical data for *MoTa* or *MoHf* have been unsuccessful, we refer again to the *MoNb* data in Fig. 7. Although slightly shifted to lower energy, $\Delta\sigma_1$ around 1.5 eV shows clearly a positive peak, which is in accord with the rigid-band-model prediction within the framework of the indirect model of optical transition. Thus the $\Delta\sigma_1$ structure around 1.5 eV in various Mo-based alloys are shown to behave consistently with the rigid-band-model prediction based on the indirect optical transition. This, in turn, supports the applicability of the indirect transition model to the optical absorption of Mo around 1.5 eV. That is, the sharp absorption edge near 1.5 eV in the optical conductivity of pure Mo results mainly from the indirect transitions originating from a peak in the density of states around 1.5 eV below the Fermi level.

Finally, we would like to point out that, in principle, the wave-vector nonconserving optical absorption should also be induced by the disorder due to thermal phonons. This point can readily be verified by looking into the experimental results of thermoreflectance measurements. In Fig. 9 thermomodulation spectra measured by Colavita *et al.*^{5,19} are shown for pure Mo and *Mo_{0.8}Nb_{0.2}* alloy in terms of $\Delta\sigma_1$. Two distinct negative peaks for pure Mo indicated by arrows in Fig. 9 apparently correspond to our

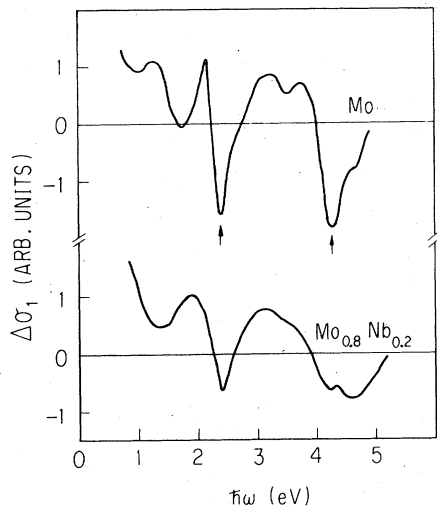


FIG. 9. Thermomodulation spectra $\Delta\sigma_1$ for pure molybdenum and a Mo-rich Mo-Nb alloy, from Ref. 5.

4.1- and 2.2-eV dips in Fig. 4. Therefore, these structures are considered as arising from wave-vector-nonconserving optical transitions induced by thermal disorder, indicating that this mechanism is also important in the analysis of thermomodulation spectra. It is interesting to note that these peaks are less pronounced in the spectrum for $\text{Mo}_{0.8}\text{Nb}_{0.2}$ alloy, indicating that the effect of thermal phonons to induce wave-vector-nonconserving optical absorption is much smaller in alloys where disorder by impurity atoms already exists. The last point, however, should not be taken as a unique interpretation, since if there is any broadening of the energy eigenvalues by any means, including impurity scattering, the thermomodula-

tion spectrum will broaden, simply because it is a derivative spectrum.

IV. CONCLUSION

We have shown that the differential optical conductivity of Mo-based alloys provides a sensitive probe to measure the change of electronic structure of Mo upon alloying. Calculations of differential optical conductivity based on both indirect- and direct-transition models were compared with the observed differential conductivity. The impurity-independent negative peaks at 4.1 and 2.2 eV in the differential optical conductivity are shown to result from the change in the optical conductivity caused by the impurity-induced wave-vector-nonconserving optical transitions, indicating that the pronounced peak near 4.0 eV and a shoulder at 2.2 eV in the optical conductivity of pure Mo consist mainly of direct transitions. Similar structures are also shown to exist in the thermomodulation spectra for pure Mo.^{5,19} The impurity-dependent structure around 1.5 eV is shown to be consistent with the rigid-band model, which suggests that the absorption edge near 1.5 eV in pure Mo results mainly from indirect optical transitions originating from a peak in the density of states about 1.5 eV below E_F . This interpretation is also shown to be consistent with the results for Mo-Nb alloys.⁴

ACKNOWLEDGMENTS

One of the authors (M.T.) would like to acknowledge Dr. D. Koelling and Dr. W. E. Pickett for their kind offer to use their original data in the analysis of the present experimental results. This work was performed in part at the University of Maryland.

¹W. L. McMillan, *Phys. Rev.* **167**, 331 (1968).

²See, for example, W. Royall Cox, D. J. Hayes, and F. R. Brotzen, *Phys. Rev. B* **7**, 3580 (1973).

³S. K. Bahl and H. D. Drew, *Phys. Status Solidi B* **74**, 721 (1976).

⁴E. S. Black, D. W. Lynch, and C. G. Olson, *Phys. Rev. B* **16**, 2337 (1977).

⁵E. Colavita, A. Franciosi, R. Rosei, F. Sacchetti, E. S. Giuliano, R. Ruggeri, and D. W. Lynch, *Phys. Rev. B* **20**, 4864 (1979).

⁶M. Tokumoto, H. D. Drew, and A. Bagchi, *Phys. Rev. B* **16**, 3497 (1977).

⁷D. Beaglehole, *Appl. Opt.* **7**, 2218 (1968).

⁸B. W. Veal and A. P. Paulikas, *Phys. Rev. B* **10**, 1280 (1974).

⁹M. M. Kirillova, L. V. Nomerovannaya, and M. M. Noskov, *Zh. Eksp. Teor. Fiz.* **60**, 2252 (1971) [*Sov. Phys.—JETP* **33**, 1210 (1971)].

¹⁰M. Tokumoto, *Phys. Rev. B* **22**, 638 (1980).

¹¹D. D. Koelling, F. M. Mueller, and B. W. Veal, *Phys. Rev. B* **10**, 1290 (1974).

¹²Neville Smith and co-workers have used an interpolation scheme to obtain matrix elements, unfortunately only on fcc metals, and they find large variations with wave vector within one band pair, and large variations between band pairs at the same wave vector. See R. L. Benbow and N. V. Smith, *Phys.*

Rev. B **27**, 3144 (1983), and references therein.

¹³C. S. Wang and J. Callaway, *Phys. Rev. B* **9**, 4897 (1974).

¹⁴C. S. Wang and W. E. Pickett, *Phys. Rev. Lett.* **51**, 597 (1983).

¹⁵D. Beaglehole and T. J. Hendrickson, *Phys. Rev. Lett.* **22**, 133 (1969).

¹⁶W. E. Pickett and P. B. Allen, *Phys. Rev. B* **11**, 3599 (1975).

¹⁷In Fig. 10 of Ref. 4, Black *et al.*, tried a similar comparison of their low-energy data with the rigid-band model calculation of Pickett and Allen for the case of 20 at. % Mo in Nb and 20 at. % Nb in Mo. However, it appears that the calculated spectra for Nb-rich and Mo-rich ends were misquoted, and comparison was made between wrong pairs of the theoretical and experimental results.

¹⁸Strictly speaking, the data in Fig. 4 are not quantitatively consistent with the rigid-band model in its simplest form, where one expects a change proportional to the number of extra electrons introduced by the impurity. After subtraction of the Drude contribution, the 1.5-eV dip grows only slightly as one goes from Re to Pt. It could be that the rigid-band model only works well for Re where the potential differences are small and for Os and Pt extra impurity states are being produced which soak up some extra electrons.

¹⁹E. Colavita, A. Franciosi, C. Mariani, and R. Rosei, *Phys. Rev. B* **27**, 4684 (1983).